Supporting Information

for

An Anionic Metal–Organic Framework For Adsorption and Separation of Light Hydrocarbons

Jia Li,[†] Hong-Ru Fu,[‡] Jian Zhang,[‡] Lan-Sun Zheng,[†] and Jun Tao*[†]

[†]State Key Laboratory of Physical Chemistry of Solid Surfaces & Department of Chemistry, College of Chemistry and Chemical Engineering, Xiamen University, Xiamen 361005, People's Republic of China

[‡]Fujian Institute of Research on the Structure of Matter, Chinese Academy of Science, Fuzhou 350002, People's Republic of China.

Tel: 86-592-2188138; Fax: 86-592-2183047. E-mail: taojun@xmu.edu.cn

Table of Contents

I) Experimental Section

Materials and Methods. Chemicals were purchased from commercial sources and were used without further purification. Thermogravimetric analysis was performed on a NETZSCH TG 209 thermobalance in a nitrogen atmosphere, sample was placed in alumina containers and data were recorded at 10 °C/min between 20 and 1000 °C. IR spectra (KBr pellet) were obtained from a Nicolet 5DX spectrometer in the region of 400–4000 cm^{-1}. Powder X-ray diffraction (PXRD) data were collected on Bruker D8 ADVANCE diffractometer at room temperature using Cu *Kα* (*λ* = 1.5418 Å) radiation. Elemental analysis of carbon, hydrogen and nitrogen was carried out on a Vario EL III analyzer. The single-crystal X-ray diffraction data were collected on an Agilent Technologies SuperNova X-ray diffractometer with Cu *Kα* radiation (λ = 1.54178 Å) at 100 K. The data were processed using CrysAlis^{pro},[1] the structure was solved and refined using Full-matrix least-squares based on F^2 with program SHELXS-97 and SHELXL-97[2] within Olex2.[3] The contribution of highly disordered solvent molecules was treated using SQUEEZE procedure implemented in PLATON program.[4] Gas sorption isotherms were performed on Micromeritics ASAP 2020 and Trist 3020 aparatus. Magnetic susceptibility measurements were carried out on a Quantum Design MPMS XL7 SQUID magnetometer in the 2−300 K temperature range under magnetic field of 1000 Oe. Magnetic data were calibrated with the sample holder, and diamagnetic corrections were estimated from Pascal's constants.

[1] CrysAlisPro, Version 1.171.35.19. (2011). Agilent Technologies Inc. Santa Clara, CA, USA.

[2] Sheldrick, G. M. (2008). A short history of SHELX. *Acta Cryst*. A64, 112-122.

[3] Dolomanov et al. (2009). OLEX2: a complete structure solution, refinement and analysis program. *J. Appl. Cryst*. 42, 339-341.

[4] Spek, A. L. *Acta Cryst*. 1990, A46, 194-201.

Synthesis of $(H_3O)_4[Ni_6(\mu_3\text{-}O)_2(\mu_2\text{-}OSC_2H_6)_2(SO_4)_2(TATB)_{8/3}]\cdot(C_2H_6O)_4\cdot(H_2O)_{13}$ [$(H_3O)_4$1·*S*]: 1) Solid $NiSO_4\cdot 6H_2O$ (0.1650 g, 0. 6 mmol) was dissolved in 5 mL DMSO; 2) 4,4′,4″-*s*-triazine-2,4,6-triyl-tribenzoic (TATB) acid (0.0441 g, 0.1 mmol)

and triethyleneamine (100 uL) was added to 5 mL EtOH and the solution was stirred 15 min to let TATB acid completely dissolve; 3) The two solutions were mixed in a 23 ml Teflon-lined stainless steel vessel, and the vessel was sealed and heated to 130 ºC within 3600 min, maintained at that temperature for another 3600 min and then cooled to 30 ºC in 2880 min. Dark yellow block crystals of the title complex were washed by EtOH and separated by filtration. Yield: ~63%. Elemental analysis (%) for $C_{76}H_{106}Ni_6O_{49}N_8S_4$: calcd: C 38.16, H 4.47, N 4.69, S 5.35; found: C 37.75, H 4.77, N 4.71, S 5.07. IR (KBr, cm^{-1}): 3412, 1612, 1566, 1520, 1384, 1356, 1101, 1016, 819, 755, 506.

II) Tables

Table S1. Crystal Data and Structure Refinements for the title complex.

Solvent-free formula	$Ni_3C_{34}H_{22}O_{14}N_4S_2$
M_r / g mol^{-1}	950.81
cryst syst	cubic
space group	$Im\bar{3}$
a / Å	26.7674(5)
V / $Å^3$	19178.7(6)
Z	12
Solvent-free D_c / g cm^{-3}	0.988
μ / mm^{-1}	2.017
reflns collected	8128
GOF	1.321
R_{int}	0.1240
R_1 ($I > 2\sigma(I)$) [a]	0.1055
wR_2 (all data)	0.2833

[a] $R_1 = ||F_o| - |F_c||/|F_o|$; $wR_2 = \{[w(F_o^2 - F_c^2)^2]/[w(F_o^2)^2]\}^{1/2}$; $w = 1/[\sigma_2(F_o^2) + (ap)^2 + bp]$, where $p = [\max(F_o^2, 0) + 2F_c^2]/3$; and $Rw = [w(|F_o| - |F_c|)^2/w|F_o|^2]^{1/2}$, where $w = 1/\sigma^2(|F_o|)$.

Table S2. Selected bond lengths (Å) and angles (deg).

Ni(1)-O(1)	1.971(4)	Ni(1)-O(6)	2.189(5)
Ni(1)-O(3)	1.969(4)	Ni(2)-O(3)	1.956(8)
Ni(1)-O(5)	2.103(4)	Ni(2)-O(2)	2.032(4)
Ni(1)-Ni(1b)	2.922(2)		
Ni(2)-O(3)-Ni(1)	115.1(2)	Ni(1)-O(5)-Ni(1b)	88.4(2)
Ni(1a)-O(3)-Ni(1)	129.7(4)	Ni(1)-O(6)-Ni(1b)	83.7(3)

Symmetry codes: a) $-x, 1-y, z$; b) $x, 1-y, -z$; c) $-x, y, -z$.

Table S3. Virial graph analysis and separation selectivity of C2 hydrocarbons over methane.

Adsorbate	T	K_H	A_0	A_1	R^2	$S_{i/j}$[a]	Q_{st}
	K	mol $g^{-1}Pa^{-1}$	ln(mol $g^{-1}Pa^{-1}$)	g mol^{-1}			kJ mol^{-1}
CH_4	273	1.320×10^{-8}	-18.142	-502.079	0.99918		17.62
	297	7.2×10^{-9}	-18.755	-392.171	0.99908		
C_2H_2	273	3.294×10^{-7}	-14.926	-893.646	0.99467	24.95	29.37
	297	1.175×10^{-7}	-15.957	-748.37	0.99767	16.32	
C_2H_4	273	1.978×10^{-7}	-15.436	-757.639	0.99658	14.98	28.62
	297	7.68×10^{-8}	-16.382	-627.907	0.99884	10.67	
C_2H_6	273	3.659×10^{-7}	-14.821	-1043.231	0.99923	27.72	27.27
	297	1.325×10^{-7}	-15.837	-810.772	0.99782	18.41	

[a] The Henry's Law selectivity for gas component i over j is calculated based on: $Si/j = K_H(i)/K_H(CH_4)$.

III) Additional Figures

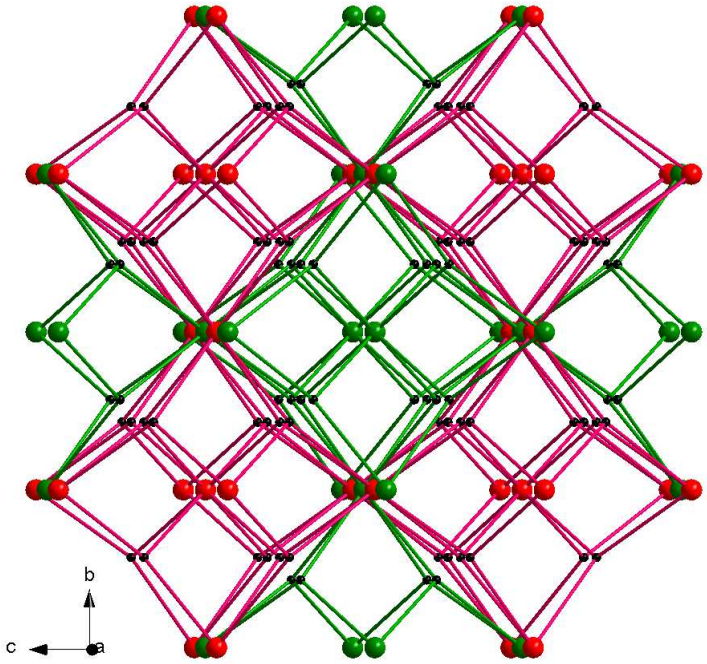

Figure S1. The two-fold interpenetrated three-dimensional topological structure. Black balls: centers of organic ligands; Green and red balls: eight-connected Ni_6 units.

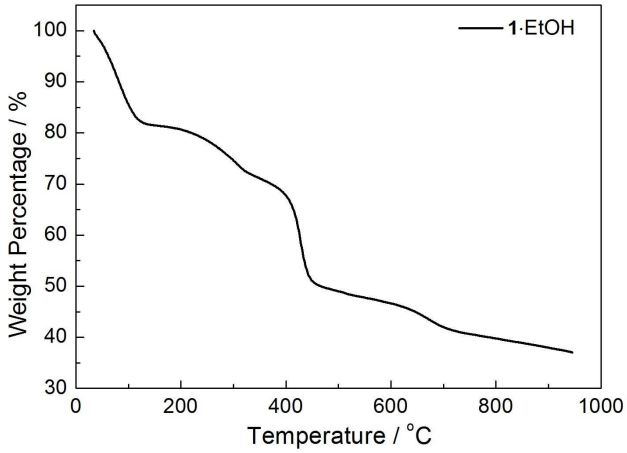

Figure S2. TGA pattern.

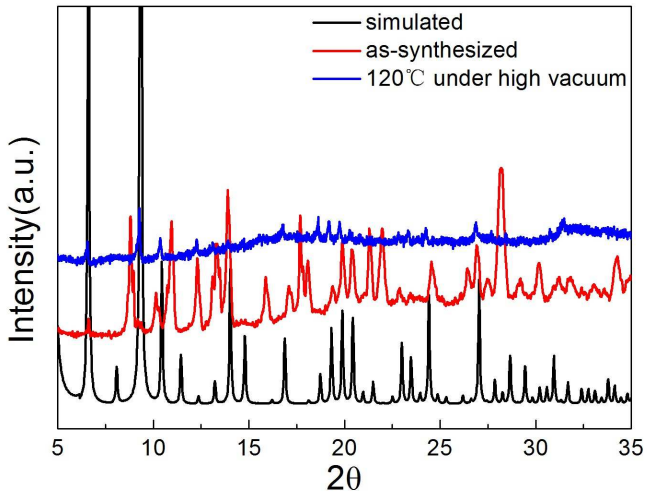

Figure S3. PXPD pattern.

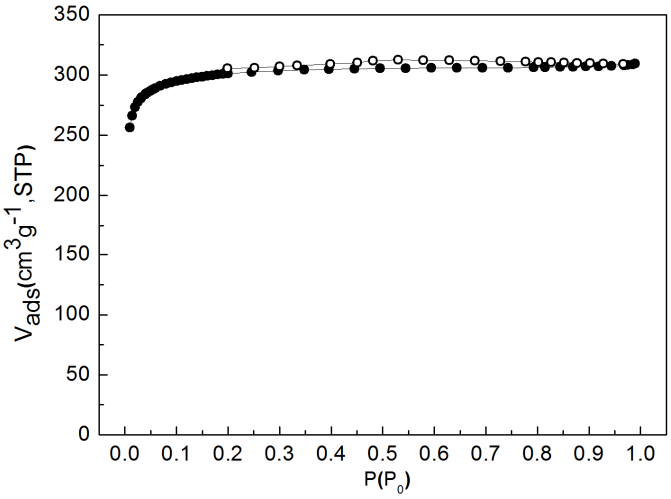

Figure S4. Nitrogen adsorption isotherms of activated sample. Full symbol: adsorption; empty symbol: desorption.

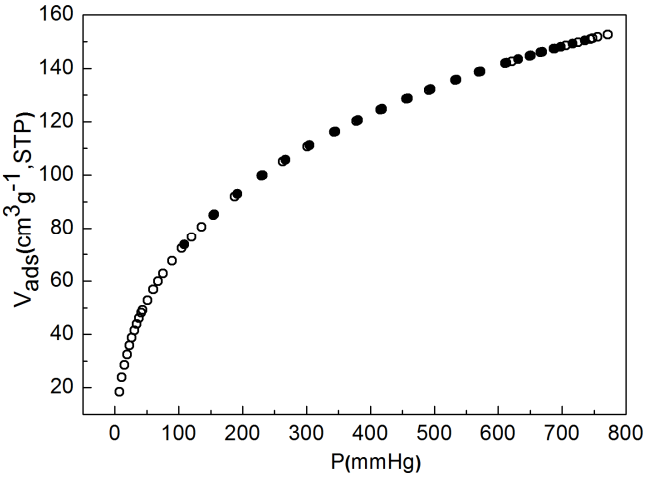

Figure S5. Hydrogen adsorption isotherms of activated sample. Full symbol: adsorption; empty symbol: desorption.

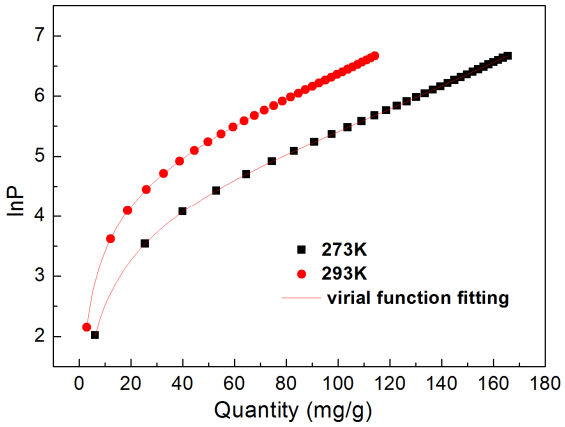

Equation	y= n(x)+1/k*(a0+a1*x+a2*x^2 +a3*x^3+a4*x^4+a5*x^5)+(b0+b1*x +b2*x^2)	
	Value	Stander Error
a0*	-3087.1902	3.44531
a1*	3.54566	0.11386
a2*	-0.05134	0.00113
a3*	-6.43757E-5	1.48649E-5
a4*	7.60615E-7	9.66257E-8
a5*	-2.0837E-9	2.25241E-10
b0*	11.46617	0.01198
b1*	-0.00807	4.00782E-4
b2*	2.05381E-4	2.97551E-6
k	273.15	0
k	297	0

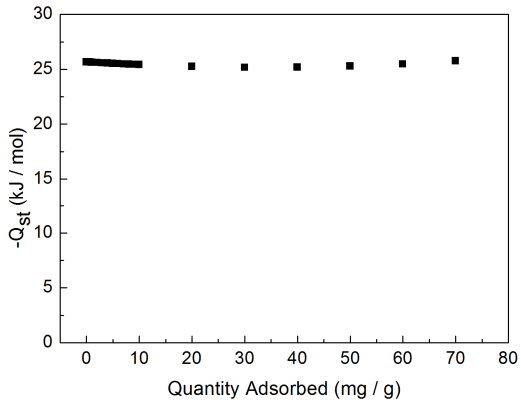

Figure S6. Virial fitting (lines) of the CO_2 adsorption isotherms (points) measured at 273 and 297 K.

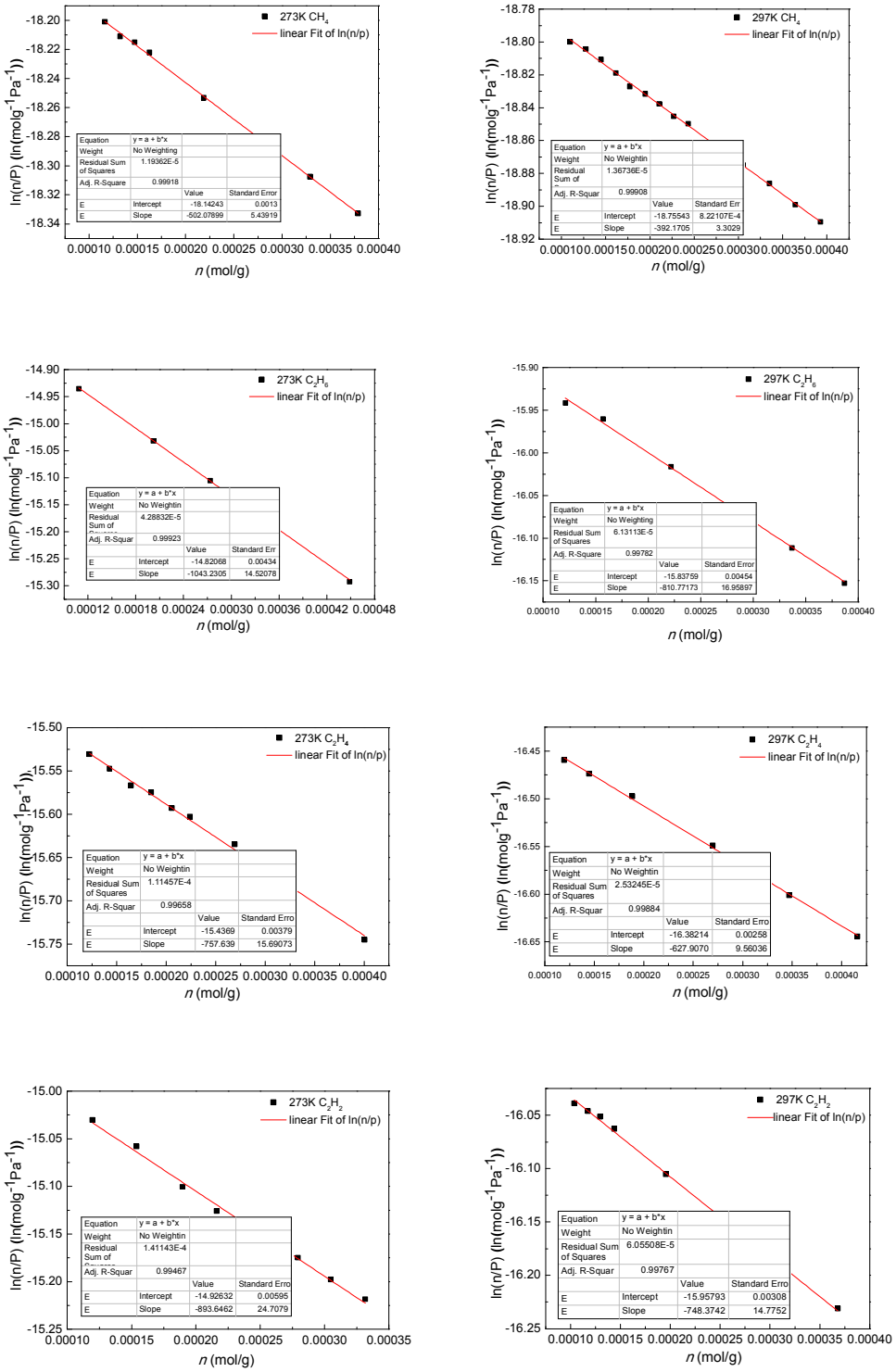

Figure S7. The virial graphs for adsorption of methane and C_2 hydrocarbons at 273 K (left) and 297 K (right).

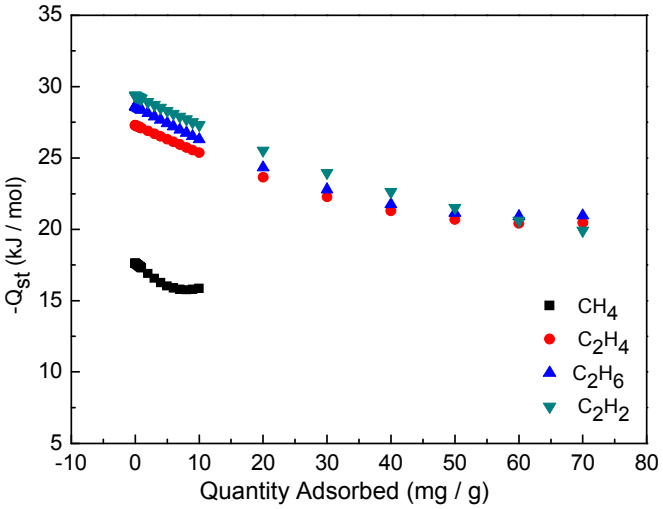

Figure S8. Virial fitting (lines) of the methane and C_2 hydrocarbons adsorption isotherms (points) measured at 273 and 297 K.

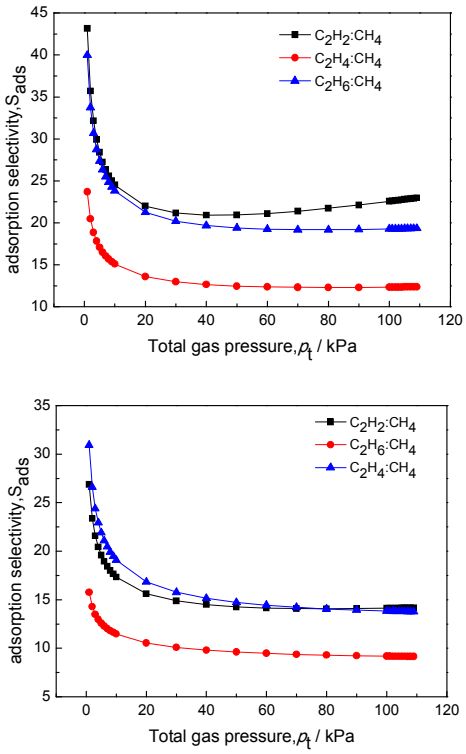

Figure S9. IAST calculations of the C_2H_6/CH_4、C_2H_4/CH_4 and C_2H_2/CH_4 adsorption selectivity for adsorption from an equimolar mixture at total bulk gas phase at 273 K (top) and 297 K (bottom).

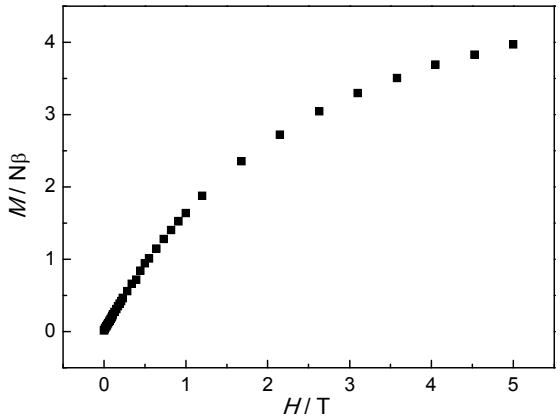

Figure S10. Field-dependent magnetization at 2 K.

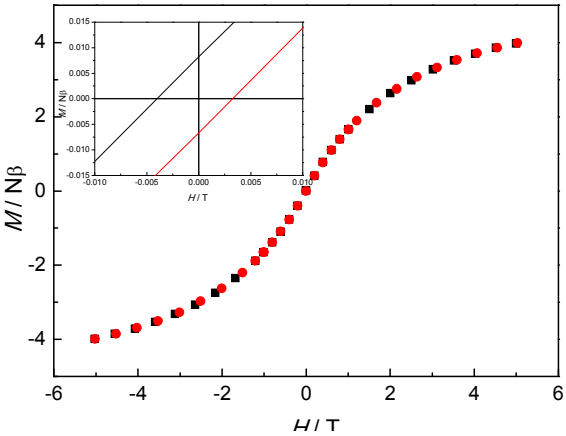

Figure S11. The hysteresis loop at 2 K.

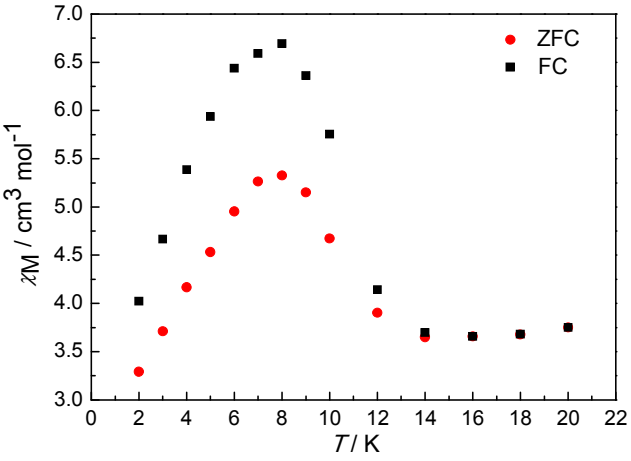

Figure S12. ZFC-FC magnetization versus temperature.

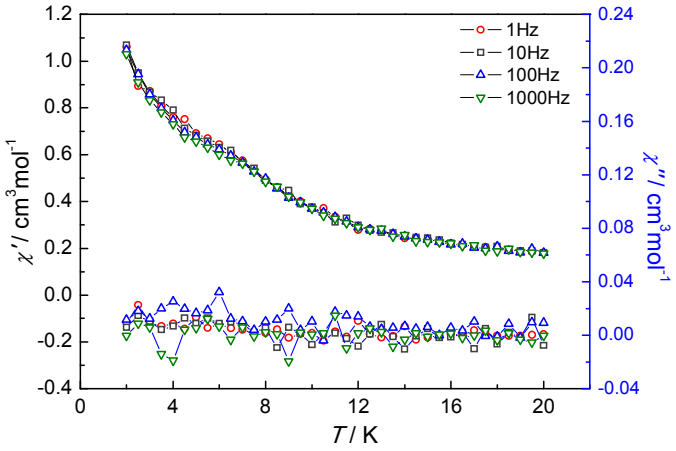

Figure S13. AC magnetic susceptibility of $(H_3O)_4$**1**·*S* under 3 Oe AC magnetic field and zero DC magnetic field.

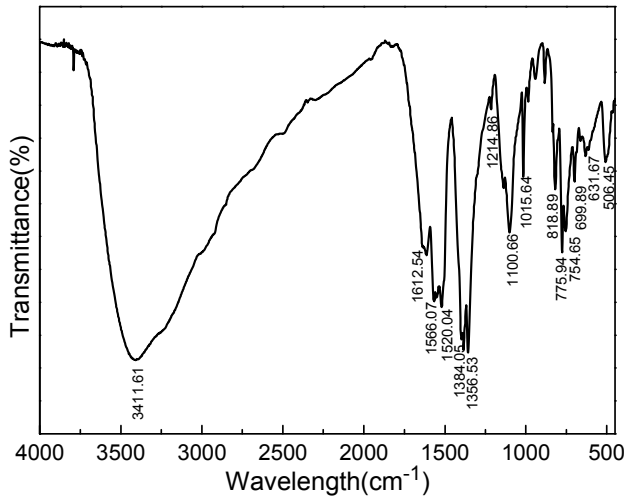

Figure S14. Infrared spectra.